nature photonics

SUPPLEMENTARY INFORMATION

DOI: 10.1038/NPHOTON.2016.207

In the format provided by the authors and unedited.

High-magnification super-resolution FINCH microscopy using birefringent crystal lens interferometers

Nisan Siegel[1,2,3], Vladimir Lupashin[4], Brian Storrie[4] and Gary Brooker[1,2,3,*]

[1]*Department of Biomedical Engineering, Johns Hopkins University, 9605 Medical Center Drive Suite 240, Rockville, Maryland 20850 USA.*
[2]*Microscopy Center, Johns Hopkins University Montgomery County Campus, Rockville, Maryland 20850 USA.*
[3]*CellOptic, Inc. 9605 Medical Center Drive Suite 224, Rockville, Maryland 20850 USA.*
[4]*Department of Physiology and Biophysics, University of Arkansas for Medical Science, 4301 West Markham St., Little Rock, Arkansas 72205*
** Corresponding author: gbrooker@jhu.edu*

Theoretical considerations of combining non-polarizing optics with birefringent lenses

A previous differential focusing beam splitting method for FINCH has used a glass lens in combination with an electrically variable GRIN lens [S1] in a total transmission-mode configuration [S2,S3]. The GRIN method has increased the light budget of the FINCH optical system while also enabling high contrast, low-aberration final processed images. While the GRIN method is an improvement over a proposed SLM glass lens combination [S4], it still is resolution limited because the desired lens phase patterns are limited by the number of graded regions used to create the liquid crystal GRIN lens. Furthermore it is challenging to make GRIN lenses that simultaneously have large clear apertures and high numerical apertures needed for high resolution imaging and compactness of a holographic system. In the GRIN lens system used to produce the comparison example shown here in Supplemental Fig. S1, the GRIN lens had approximately a 5000 mm focal length and the glass lens a 300 mm focal length. This combination of focal lengths creates a spacing factor between the two focal lengths of less than 3% (f_{d1} ~284 mm and f_{d2} ~300 mm), which reduces the axial depth of 3D object space that can be reliably imaged by the holographic system [S2,S3,S5]. So while the GRIN method negates some of the disadvantages of the SLM methods, it is significantly less flexible in terms of the choices available for z_h and s. Furthermore, while the aberrations of the SLM methods are avoided, the GRIN lens uses clear conductive elements to apply the electrical control to the liquid crystal orientation to achieve the graded index effect. These conductive elements do not modulate the beam with the desired spherical phase and in fact impart some diffraction artifacts to both the modulated and unmodulated transmitted beams.

Equivalently to using a solid birefringent crystal, a birefringent liquid crystal material may be used to create a birefringent lens when suitably aligned between two substrates with curvatures R_1 and R_2. By virtue of the extraordinary axis of the birefringent crystal being orthogonal to the direction of light propagation, the extraordinary axis will not impart a transverse offset to the beam as can happen in other axis orientations. And as spherical lenses, birefringent lenses will display none of the diffractive defects listed above for SLMs and GRIN lenses, with only the usual refractive lens aberrations that can be mitigated by appropriate optical design. The two focal lengths of the birefringent lens may then be used as the two focal lengths necessary for the holographic process; i.e. f_{be} and f_{bo} may be substituted for f_{d1} and f_{d2} in equations 1 and 2 in the main text. Then, any single lens made of a given type of birefringent material will have a constant spacing factor no matter the effective curvature R_{eff}^{BRL} of the lens:

$$s = \left|\left(n_o - n_e\right)/\left(n_o + n_e - 2\right)\right|. \qquad \text{(S1)}$$

This also implies that the hologram distance z_h of optimal overlap is dictated simply by the choice of birefringent lens material and effective curvature:

$$z_h = 2R_{eff}^{BRL} / \left(n_o + n_e + 2\right). \qquad \text{(S2)}$$

However, when used in conjunction with a non-birefringent lens (see main text Fig. 2(c)), each of the focal lengths of the birefringent lens combines with the single focal length f_r of the non-birefringent lens to result in two new combined focal lengths. Under the thin-lens approximation and assuming no distance between the birefringent lens and the standard lens, the focal lengths f'_{be} and f'_{bo} of the combined system are now:

$$\begin{aligned} f'_{be} &= f_{be} f_r / \left(f_{be} + f_r\right) \\ f'_{bo} &= f_{bo} f_r / \left(f_{bo} + f_r\right) \end{aligned}, \qquad \text{(S3)}$$

and the combined spacing factor s' of the hologram system can be increased and decreased from the constant value in equation S1 according to the following equation:

$$s' = \left| \left(n_o - n_e\right) / \left(n_o + n_e - 2 + 2R_{eff}^{BRL} / f_r\right) \right|. \qquad \text{(S4)}$$

The corresponding modified expression for optimal hologram distance z'_h is:

$$z'_h = 2R_{eff}^{BRL} / \left(n_o + n_e + 2R_{eff}^{BRL} / f_r\right). \qquad \text{(S5)}$$

Note the similarity of equations S4 and S5 to equations S1 and S2, showing the additional factor for adjustment based on the ratio of the birefringent lens effective curvature and the classical glass lens focal length. Thus it can be seen that a wide range of independently varying spacing factors and hologram distances may be obtained by appropriate combinations of birefringent lenses with classical non-birefringent lenses. For example, by referring to the last term in the denominator of equation S4, it can be seen that a reduction in spacing factor s can be obtained by use of a negative birefringent lens with a positive classical lens. Additionally, in the case of lens combinations, chromatic aberrations may also be addressed in the design of the compound birefringent/classical lens system.

Results of fabrication of birefringent lenses

Calcite: Calcite has refractive indices of $n_e = 1.48$ and $n_o = 1.66$, leading to predicted values of $f_{be} = 194$ mm and $f_{bo} = 263$ mm for $R_{eff} = 127$ mm. The observed focal lengths, as measured by a Shack-Hartmann wavefront sensor, were 184 and 230 mm. This suggests that the curvature of the lens may not have been exactly at specification, but does not affect the overall concept of the work. The observed focal lengths lead to $z_h = 204$ mm and $s = 0.11$.

α-BBO: The α-BBO lens was designed for use along with a standard glass lens as described in equations S3-5. A negative curvature was selected in order to increase the spacing factor beyond that of the GRIN-based systems to about 5%. Assuming the refractive indices of α-BBO are equal to those of β-BBO as $n_e = 1.55$ and $n_o = 1.68$ leads to predicted values of $f_{be} = -804$ mm and $f_{bo} = -985$ mm for $R_{eff} = -545$ mm. When this lens was coupled with a 250 mm achromat, focal planes were observed with $f_{be} = 335$ mm and $f_{bo} = 366$ mm, close to the values predicted by eqn. S3. Therefore for α-BBO-FINCH $z'_h = 349$ mm and $s' = 0.04$.

Imaging the USAF pattern at low magnification/low NA

The first fluorescence microscopy experiment with α-BBO-FINCH was performed on the standard fluorescent USAF pattern using a 20× 0.75 NA Nikon objective. As can be seen in Supplemental Fig. 1, the α-BBO-FINCH recovered object phase (Supplemental Fig. 1a) is well modulated and the modulation depth between the finest features of the USAF pattern is much deeper for the α-BBO-FINCH image (Supplemental Fig.1b,d) than for the classical image (Supplemental Fig. 1c,e). This indicates that the performance of birefringent lens-based FINCH for real extended incoherent objects matches that of SLM and GRIN based FINCH at lower magnifications.

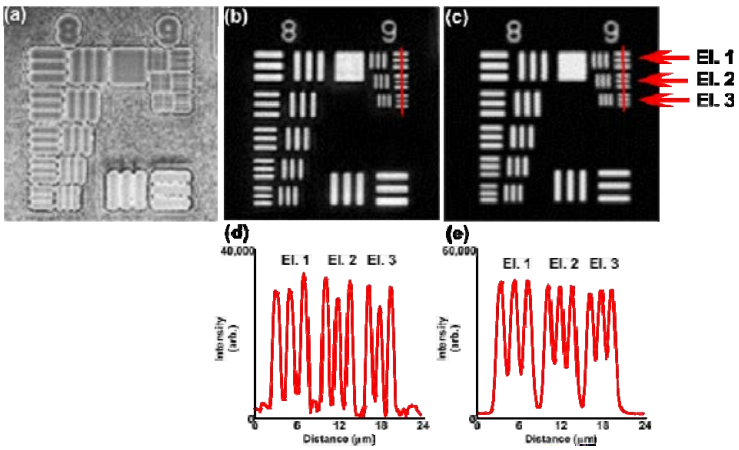

Supplemental Figure S1. USAF fluorescence images taken with α-BBO-FINCH and classical widefield microscopy. (a) Complex hologram phase, (b) and (d) reconstructed FINCH image and indicated intensity line profile, (c) and (e) classical wide-field image and intensity profile. Object field of view is 67 μm.

Comparative images of HeLa cell Golgi proteins imaged with a commercial SIM instrument

Our results were compared to those obtained with a leading commercial structured illumination (SIM) microscope. An example image from that microscope using the same fluorescent probes in HeLa cells is shown in Supplemental Fig. 2 for comparison to the results obtained with α-BBO FINCH (see main text Fig. 5). Optimal results with SIM required twenty-five 100 ms image captures per colour, while with FINCH, only three phase-shifted 100 ms image captures per colour were required.

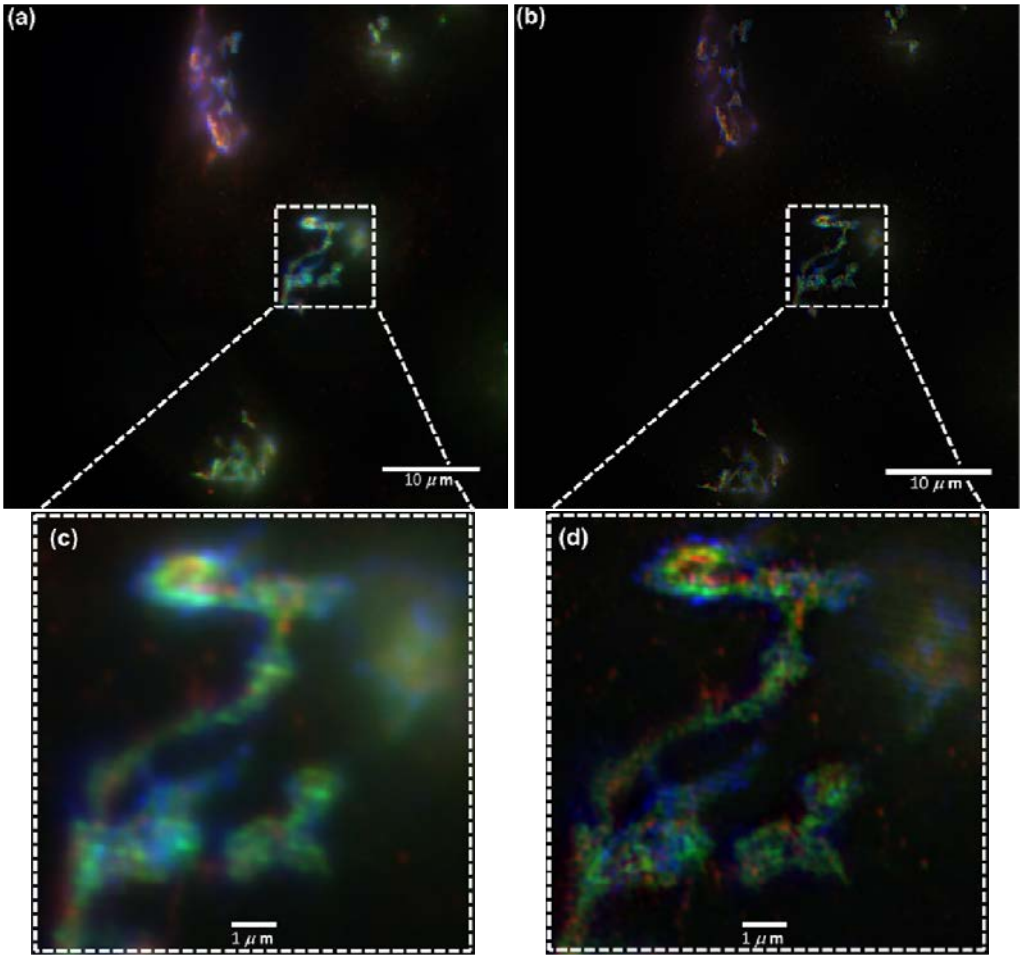

Supplemental Figure S2. Three HeLa cell Golgi apparatus fluorescently labeled proteins imaged with a commercial SIM instrument in widefield mode (a) or SIM mode (b). The proteins were labeled with GalT-GFP (green), and two other Golgi proteins TGN46 and GM130 immunolabeled and respectively stained with DyLight549 (blue) and DyLight647 (red) as in Fig. 5 of the main text. The SIM image was obtained after 25 images per colour were captured (100 msec capture time per image) at the excitation wavelength for each dye and the images processed by the instrument software. Images (c) and (d) are corresponding enlarged 10 micron square selections respectively. A Zeiss alpha Plan-Apochromat 100X super resolution 1.46 NA oil DIC objective was used.

References

S1. Hashimoto, N. & Kurihara, M. Liquid crystal quantized GRIN lens and its application to AF systems. *Proc. SPIE Emerg. Liq. Cryst. Technol. IV* 7232, 72320N–72320N–8 (2009).

S2. Brooker, G. *et al.* In-line FINCH super resolution digital holographic fluorescence microscopy using a high efficiency transmission liquid crystal GRIN lens. *Opt. Lett.* **38**, 5264–7 (2013).

S3. Siegel, N. & Brooker, G. Improved axial resolution of FINCH fluorescence microscopy when combined with spinning disk confocal microscopy. *Opt. Express* **22**, 22298–307 (2014).

S4. Rosen, J., Siegel, N. & Brooker, G. Theoretical and experimental demonstration of resolution beyond the Rayleigh limit by FINCH fluorescence microscopic imaging. *Opt. Express* **19**, 26249–68 (2011).

S5. Siegel, N., Rosen, J. & Brooker, G. Reconstruction of objects above and below the objective focal plane with dimensional fidelity by FINCH fluorescence microscopy. *Opt. Express* **20**, 19822–35 (2012).